The Terrestrial Planet Finder Coronagraph Dynamics Error Budget

Stuart Shaklan[1], Luis Marchen, Joseph J. Green, Oliver P. Lay
Jet Propulsion Laboratory,
California Institute of Technology

ABSTRACT

The Terrestrial Planet Finder Coronagraph (TPF-C) demands extreme wave front control and stability to achieve its goal of detecting earth-like planets around nearby stars. We describe the performance models and error budget used to evaluate image plane contrast and derive engineering requirements for this challenging optical system. We show that when the coronagraph is coupled to an 8th-order band-limited mask, the performance is limited by shearing of the starlight beam across imperfect optics (a.k.a. beam walk), and that this in turn demands tight rigid body pointing, sub-milliarcsecond fine guiding, high-quality optics, and sub-micron positional stability of the optics including the secondary mirror. Additionally we show that the stability of low-order aberrations (focus, astigmatism, coma, and trefoil) is required to be ~ 2-4 Angstroms, while higher-order modes must remain stable to a few picometers.

Keywords: coronagraph, telescope, error modeling, error budget, extrasolar planets

1. INTRODUCTION

The Terrestrial Planet Finder Coronagraph[1] (TPF-C) is an 8-m space-based observatory capable of directly detecting and characterizing starlight reflected from terrestrial planets orbiting nearby stars. The observatory is required to find earth-like planets in the so-called "habitable zone," where liquid water can exist, covering roughly 0.7 – 1.5 AU from a solar-type star. At greatest elongation (quadrature), an earth-like planet in a 1 AU orbit around a solar-type star 10 parsecs away appears 100 milli-arcsec (mas) from the star, with a flux relative to the star of 4.6×10^{-10} (23.343 magnitudes fainter). The brightness decreases as the square of the semi-major axis and increases up to π times above quadrature when the planet is fully illuminated, assuming a spherical Lambertian reflectance model[2].

The instrument behind the TPF-C telescope consists of a wave front control system followed by a band-limited Lyot coronagraph[3]. The wave front is flattened to sub-Angstrom levels by a large-format, small stroke deformable mirror (DM). The baseline DM is a 96x96 actuator Xinetics device similar to the 64 x 64 devices delivered to the TPF High-Contrast Testbed[4]. The DM controls scattered light over a range of spatial frequencies, from 0 to 48 cycles/aperture. Within this range, the residual scattered light level must be driven down to a level below the expected planet flux, i.e. ~ 1e-10. In practice, this 'dark hole,' with scattered light characterized by speckles similar to laser speckle, has both an inner and outer working angle (IWA and OWA): the IWA exists because the required dynamic range for the wave front control approaches 1e10 near the core of the PSF, compared to ~1e7 at the third Airy ring. The OWA is slightly inside the Nyquist frequency of 48 cycles/aperture.

Brown has studied a list of TPF candidate stars and has determined that the IWA required to achieve the (still flexible) TPF goals is ~ 60 mas[2,5]. He has also shown that the residual instrument light level in the dark hole should have a stability better than ~1e-10/SNR, where SNR is the instrument-systematic-limited signal-to-noise ratio. We require SNR = 5, so that the stability of speckles in the dark hole is required to be < 2e-11 of the incident star light.

We have adopted a 'set and forget' approach to wave front control. In this approach, the wave front is controlled once at the beginning of an observation, and is required to remain stable for the duration T of the observation. This approach places demanding requirements on the system since observations can be long (~ 1 day) and stability requirements are extremely challenging, as will be shown below. However, a set-and-forget approach is straightforward to model – we can define clear engineering requirements for well-defined periods. The requirements are not blurred by various control

[1] Contact information: Address: 4800 Oak Grove Drive, Pasadena, CA 91109. e-mail: Stuart.Shaklan@jpl.nasa.gov

bandwidths, and they are not relaxed by as-yet unproven high-dynamic range wave front control. In the future, once detailed end-to-end models of active wave front control demonstrate the ability to reduce speckles to a level of 1e-10 and estimate their value to 2e-11, we will consider changing to an active approach and subsequently relaxing temporal stability requirements.

We thus assume the TPF observation scenario consists of the following steps: 1) Point the observatory at the target; 2) Allow the dynamics to settle and the system to reach an adequate level of thermal equilibrium; 3) Set the wave front and control the dark hole level to 1e-10; 4) Observe the target for half the time T/2 required to obtain SNR = 5; 5) Rotate 30^o about the line-of-sight (LOS); 6) Observe again for T/2 time; 7) Rotate the observatory 60^o about the LOS and repeat steps 2-6; 8) Rotate another 60^o and repeat steps 2-6. The 30^o roll, which we call a 'dither,' is used to form two nearly identical speckle patterns that can be differenced to reveal a planet near the star in two different azimuthal positions. The 60^o rolls provide azimuthal sensitivity at the IWA in regions that are blocked by the linear or elliptical-shaped coronagraph mask[6]. The dithers require the speckles to remain stable to 2e-11. The rolls are new independent observations for which a dither pair will be formed. Thus the wave front can be reset (a return to step 2) for each roll orientation and we assume that the stability requirements apply only for the time required to set the wave front and perform the two dither observations at a given roll.

2. REQUIREMENTS

The contrast error budget (CEB) specifies the level and stability of scattered light in the dark hole. The scattered light level is expressed in terms of instrument contrast, where contrast is defined as the integrated scattered light in a diffraction-limited resolution spot, normalized by the coronagraph mask throughput, and divided by the light from the star that would be present without a coronagraph mask. A rigorous definition is given in Green & Shaklan (2003)[6]. Table 1 gives the working requirements as of June, 2005.

Table 1. TPF-Coronagraph Contrast Error Budget Requirements.

	Requirement	Comment
Static Contrast	6.00E-11	Coherent Terms
Contrast Stability	2.00E-11	Thermal + Jitter
Instrument Stray Light	1.50E-11	Incoherent light
Inner Working Angle	4 λ/D_{long}	57 mas at λ=550 nm, D_{long} = 8 m
Outer Working Angle	48 λ/D_{short}	1.5 arcsec at λ=550 nm, D_{short} = 3.5 m
Bandpass	500-800 nm	Separate observ. in three 100 nm bands.

The contrast level and stability are both functions of position in the image plane. We have found that the dynamic evolution of low-order aberrations and the predominance of low-order imperfections in the optics have their largest impact at the IWA. In the rest of this paper, we evaluate the contrast error budget at the IWA. The dynamic (though not necessarily the static) contrast levels are smaller at larger working angles. We have not yet performed a detailed study of contrast stability at the OWA, though it is expected to be small compared to the IWA.

Our work over the last 3 years has led us to conclude that it is impractical to work within 3-4 λ/D (~ the third Airy ring) because as one removes diffraction at smaller working angles, the Lyot aperture is reduced while aberration sensitivity increases. Our work on aberration sensitivity (refs. 6,7, and 8) shows that for band-limited masks[3], the combination of reduced Lyot throughput and increased aberration sensitivity drives stability requirements (wave front shape change per unit time) up by ~ 1 order of magnitude when moving from 3 to 2 λ/D, and a factor of 4 between 4 and 3 λ/D.

Our inner working angle of 4 λ/D represents a compromise between the required resolution (~ 60 mas), the largest aperture that can fit in an existing launch shroud, and the engineering requirements at the IWA.

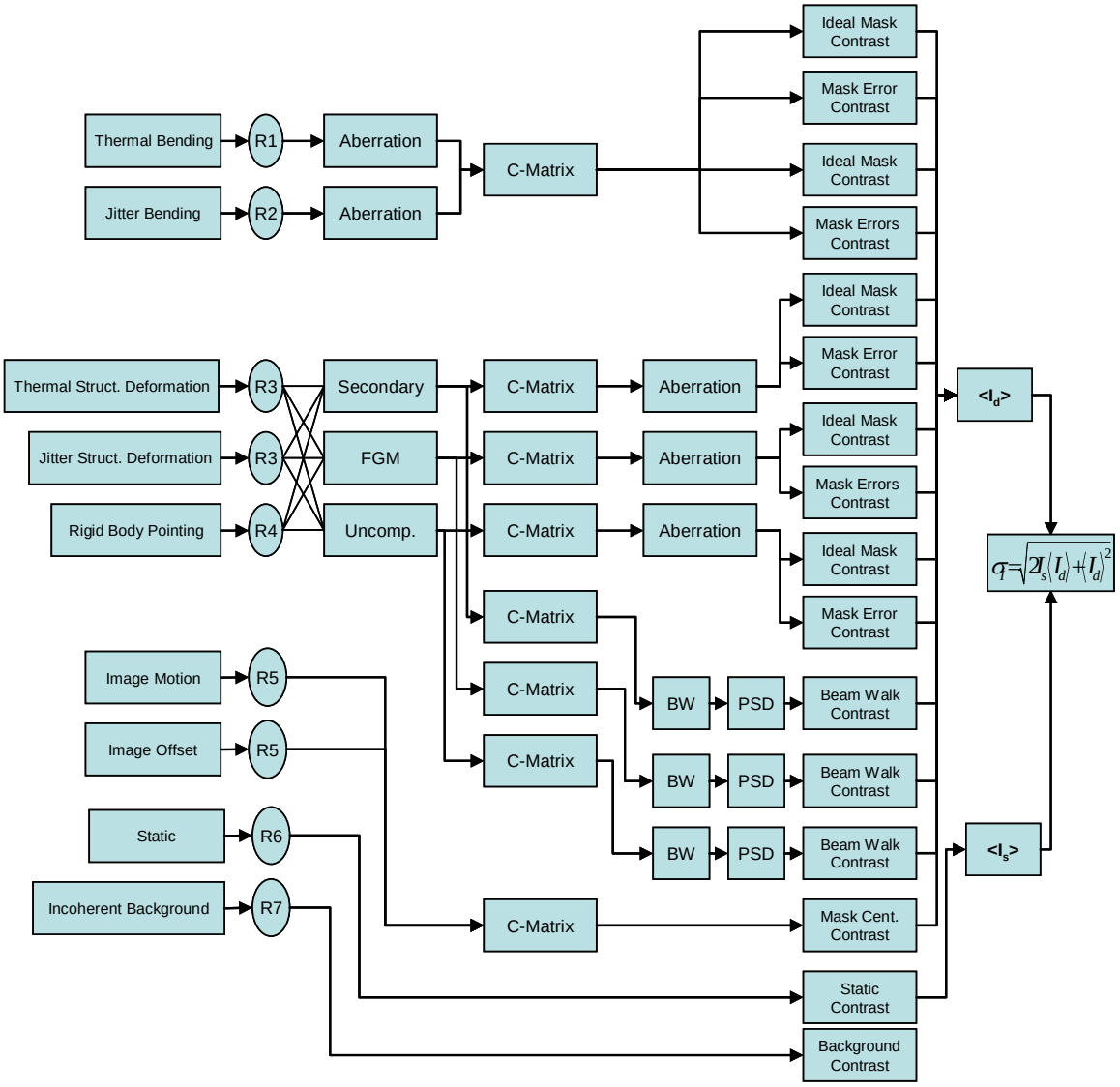

Figure 1. Error Budget Structure. 'C-matrix' is a sensitivity matrix or equation. R1-R7 are multiplicative reserve factors.

4. STRUCTURE

The CEB rolls up the allocations for individual error contributions into an observatory system contrast. It is iterated regularly to reflect changing design baselines and system understanding. It is used to manage the allocation of challenging requirements between system components and to manage the reserve margins on each of those allocations. The CEB exists as a set of Excel spreadsheets utilizing data from several models described in Sect. 5.

The CEB comprises the static (initial wavefront setting and stray light at the start of an observation) and dynamic (any changes to the wavefront during an observation) terms that contribute to image plane contrast. Static terms include wavefront sensing and control, stray light, coronagraph mask imperfections, and polarization leakage. Dynamic terms include motion of an optic or bending of an optic due to vibrations or thermal effects, and line-of-sight pointing fluctuations. Figure 1 shows the structure of the error budget including reserve factors, mean image plane contrast, and the standard deviation of contrast as detailed below.

Initial work has focused on the dynamic (thermal and jitter) part of the error budget for two reasons. First, dynamic terms are used to set requirements on modal behavior, from which design constraints follow, e.g. stiffness and thermal isolation requirements. With dynamic requirements in hand, the TPF-C design team has been able to proceed with a design that can be modeled, compared to requirements, and iterated. Static requirements, on the other hand, drive technology, e.g. the approach to wavefront sensing and control, optical manufacturing, contamination control, and high-dynamic range baffling, among other things. Second, dynamic models are largely based on linear sensitivity matrices which are simple to develop and test. These are explained in detail in Sect. 5. In contrast, modeling of static wavefront contributors involves computer intensive diffraction propagations, electromagnetic modeling of mask transmission, and requires a broad-band wave front control algorithm to compensate for scattered light. This modeling is now underway and will be folded into the error budget studies.

Dynamic Terms

Dynamically induced errors constitute optical aberrations, beam walk and image motion. Aberrations arise as the system is perturbed from its ideal design, independent of the quality of the optics. Aberrations result from bending of optics (the primary mirror is of greatest concern), as well as from structural deformation. When the structure deforms, the secondary mirror moves relative to the primary mirror, as do downstream optics. This introduces low-order aberrations that scatter light near the inner edge of the dark hole. Aberrations contribute to contrast in two ways: first, in the case of the ideal mask and Lyot stop, the mask and stop act as a spatial filter that passes a fraction of the light to the image plane. Second, mask transmission and phase errors allow aberrated light through the system, as if there was a light source located at the position of the mask error.

Beam walk is the motion of the beam across the optics. Both rigid body pointing errors and structural deformation cause the beam to be deflected from its initial state at the beginning of an observation. When the beam reaches the deformable mirror (DM), it contains wave front corrugations that are shifted with respect to the compensating corrugations on the DM. The resulting wavefront adds to the scattered light level. The phase deviation of the uncompensated wavefront varies linearly with displacement and spatial frequency, while the scattered energy varies as the square of the wavefront error[9].

In addition to aberrations and beam walk, one other dynamic term contributes to image plane contrast. This term is labeled ‘image motion’ and is the energy that leaks around the mask when the beam is not perfectly centered on it. For the 8th-order Lyot coronagraph[8,10] that we have baselined, the mask intensity leakage is proportional to the 8th power of wavefront tilt, as discussed in Sect 6.

Control Systems

Two control systems are represented in the CEB. The first is a multi-tiered pointing control system (Fig. 2). We assume that the pointing errors are measured on a high-precision camera located in the coronagraph. This camera has yet to be designed, but might utilize light reflected from the coronagraph mask or measure the distribution of light diffracted around the Lyot stop. The high-frequency pointing is compensated by a fine-guiding mirror (FGM) at or near a pupil image in the coronagraph. This mirror is desaturated by tip-tilt motion of the secondary mirror, which in turn is desaturated by the spacercraft’s reaction wheels or other pointing control mechanism. The CEB makes no assumptions about bandwidth but does assign a pointing residual to each subsystem. Our spreadsheet contains two switches allowing us to turn the secondary and FGM on and off while automatically redistributing residual pointing errors to the appropriate sensitivity matrices. The residuals will be reallocated to match the predicted subsystem bandwidths and disturbances once the dynamics modeling has been performed.

The second control system maintains the relative positions (plus pointing offsets) between the primary and secondary mirrors. Position measurements are based on a SIM-like[11] 6-beam laser metrology system[12]. We assume that the metrology system has adequate bandwidth to compensate for thermal errors but is too noisy to compensate jitter. We note that the change from a 4th-order to an 8th order coronagraph mask has relaxed the secondary positional stability requirements (and laser metrology precision requirements) by 2 orders of magnitude compared to our earlier study[12].

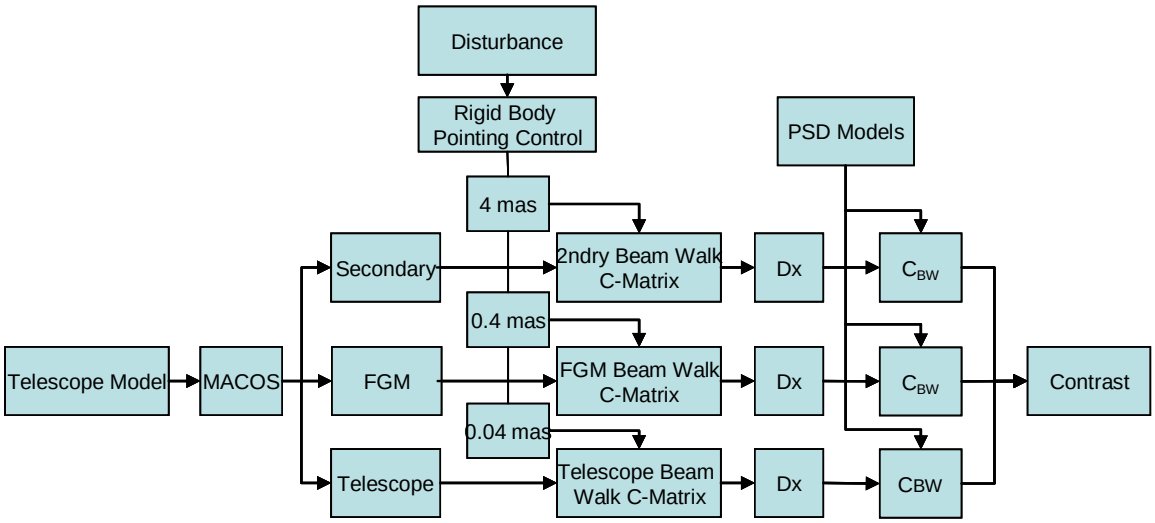

Figure 2. Pointing control. The CEB assumes a nested pointing control system. Reaction wheels and/or a Disturbance Reduction System control rigid body motions to 4 mas (1 sigma). The telescope secondary mirror tips and tilts to compensate the 4 mas motion but has a residual due to bandwidth limitation of 0.4 mas. A fine guiding mirror in the SSS likewise compensates for the 0.4 mas motion leaving 0.04 mas uncompensated.

Allocations and Reserves

The error budget allocation process begins with a first order sensitivity analysis. Engineering judgment is used to partition allowable errors throughout the subsystems. In some cases, the allocations point directly to the difficult requirements, such as the primary mirror stability, while in others requirements are derived indirectly through engineering analysis, as is the case for temperature stability requirements on the primary mirror. Reserve factors are allocated for each source and account for the performance reserve, the modeling uncertainty factor and the error in the modeling. The modeling uncertainty relates to aspects of the model which do not accurately reflect physical behavior while the modeling error refers to inaccuracies in the as-built model or physical properties. These reserve allocations are initially chosen based on engineering judgment and over time modified to reflect bounding of model calculations via testbed results. Presently, the reserve factors R1 – R7 (fig. 1) are all set to 2. In practice, the modeling activity carries additional model uncertainty factors of 3 and 10 for low- and high-order modal amplitudes, respectively.

5. MODELS

The error budget is built upon several models, as shown in Figure 3. Static models describe the optical performance of various algorithms and optical effects (e.g. stray light) that are independent of dynamic effects. Dynamic models describe the change in wavefront and contrast leakage that occur when the state of the system changes. Dynamic models used to compute the error budget include:

- A Fraunhofer pupil-to-image plane model is used for calculating image plane contrast as a function of wavefront components for ideal coronagraph designs as well as coronagraphs with mask transmission errors. The wavefront components are decomposed into Zernike polynomials that are orthogonal over circular and elliptical apertures. This is called the 'diffraction aberration sensitivity' model.

- A MACOS[13]-based aberration sensitivity model determines the Zernike mode amplitudes when any optical component is moved over 6 degrees of freedom (DOF). This model is the 'Zernike sensitivity matrix.' The telescope and coronagraph optics are described in separate papers[14,15].

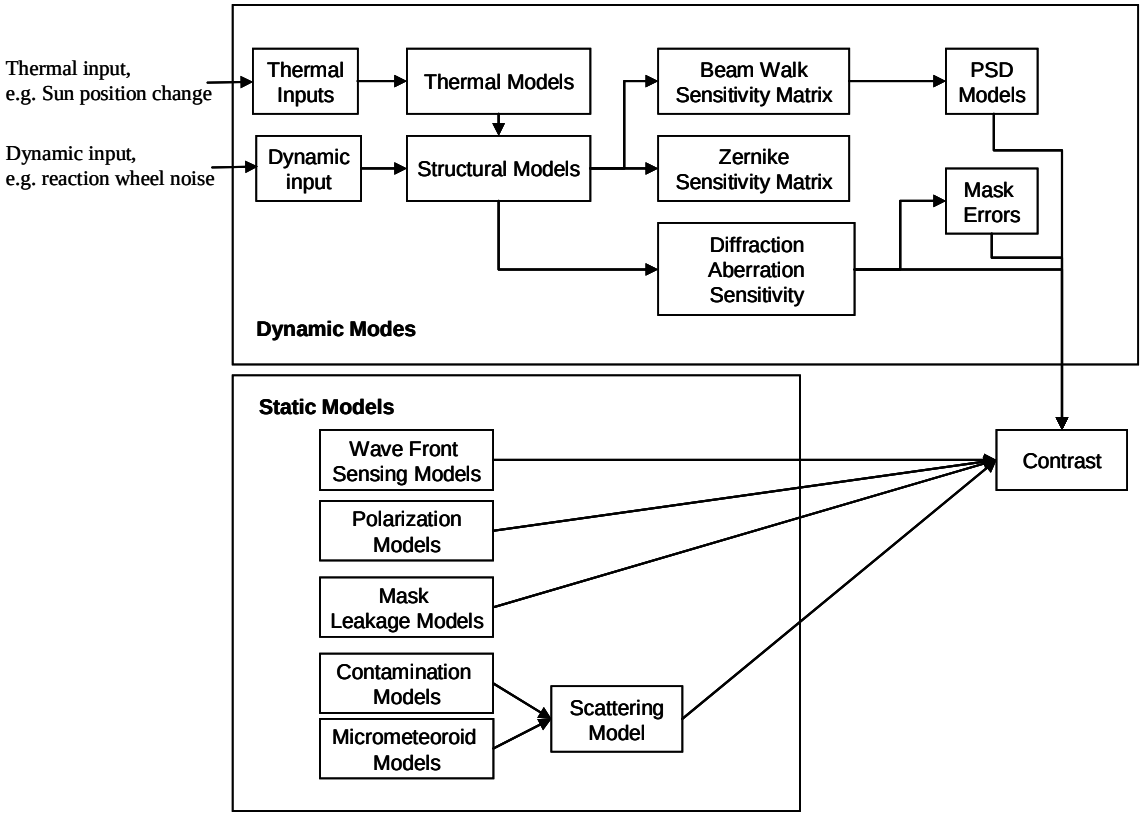

Figure 3. Models used to calculate static and dynamic contrast.

- A 'Beam walk sensitivity matrix' computed by MACOS multiplies the power spectral density (PSD) models of the optics, and is described in detail by Noecker in this conference[9]. To compute the beam walk contribution at a specific point in the image plane, the PSD is filtered by the spatial frequency corresponding to the image plane position (e.g. at 4 λ/D, the relevant frequency is 4 cycles/aperture). The amplitude of the filter is set by the lateral beam walk amplitude, which is determined by a MACOS ray trace (the 'structural model'). The PSD function we use is flat below a turnoff spatial frequency and decreases as f^{-3} above that frequency. The PSD amplitude and turnoff frequencies are selected for the primary, secondary, small flat, and small powered optics (Table 2). The PSD of the DM is the summed PSD of the other optics in the system in front of the mask (for the critical spatial frequencies comprising the 'dark hole') since its wavefront is set to be equal and opposite to the summed wavefronts of the other optics. Its roll-off parameter of 320 cycles/m is scaled by the ratio 10 cm / 8 m from the primary mirror value of 4 cycles/m. Figure 4 shows how beam walk contrast is calculated by combining the output of the MACOS linear sensitivity matrix with the contrast coefficient for a given amount of beam walk.

- The model of the laser metrology system between the primary and secondary mirrors is based on a simple linear point-to-point analysis of the metrology beams to determine beam length sensitivity to the 6 degree-of-freedom (6-DOF) motion of the secondary. We use ray tracing of the TPF-C telescope to determine aberration sensitivity versus motion of the secondary mirror. These two models are combined to yield the aberration sensitivity versus metrology beam lengths. The coronagraph model determines image plane contrast as a function of aberrations. We can thus determine by combining the linear and coronagraph models, the image plane contrast versus metrology beam length deviations[12].

- Static error models, as noted above, are based on Fresnel diffraction analysis and include broad-band multi-DM wave front control systems. Coronagraph mask errors include phase and amplitude transmission errors

measured in the laboratory[16], and theoretical models based on detailed electromagnetic calculations of mask transmission (for binary masks)[17]. We have also modeled the expected distribution of micrometeoroid damage to the primary mirror. We are currently studying scatter from particle contamination to determine what fraction of the forward and backward scattered light can be compensated by the DMs. Standard polarization ray-tracing is used to determine polarization amplitude and phase non-uniformity in the off-axis system[18], but we have not yet performed modeling of polarization effects arising from coating non-uniformities[19]. The full scope of these models and the details of the static error budget will be the subject of a future paper.

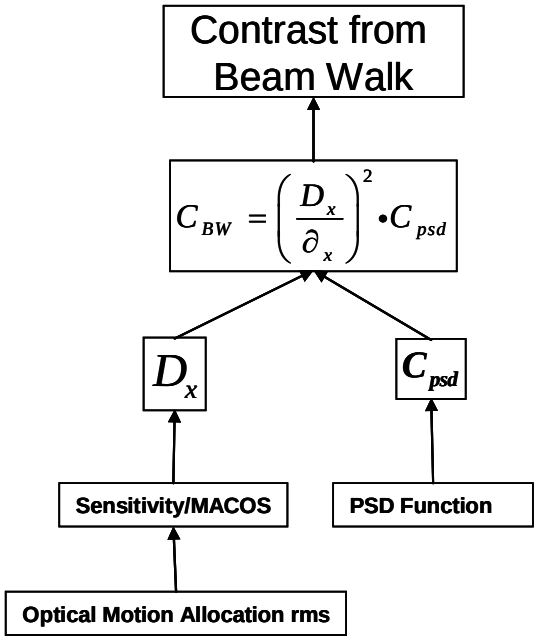

$$C_{psd} = \left(\frac{2\pi}{\lambda} \bullet \sqrt{\iint 16\pi^2 (\delta_x k_x)^2 \bullet \left[\frac{A}{1 + \left(\frac{\sqrt{k_x^2 + k_y^2}}{k_0} \right)^n} \right] dk_x dk_y} \right)^2$$

Figure 4. Beam walk calculation. C_{psd} is the contrast for a unit value of beam walk, δ_x at a spatial frequency (image plane position) of k_x.. D_x is the beam walk calculated from linear sensitivity matrices applied to allocated translation and tilt motions.

Table 2: PSD specifications for optics modeled in the CEB.

	Primary	Secondary	Fold	Super Fold	OAP	Super OAP	Anamorphic 1	Anamorphic 2	DM
D (m)	8.02	0.83	0.1	0.1	0.1	0.1	0.23	0.10	0.10
k0 (cy/m)	4	4	10	10	10	10	10	10	320
A (m^4)	9.60E-19	9.60E-19	1.25E-20	7.58E-21	1.25E-20	1.09E-20	5E-20	7.5E-20	8.52E-22
n	3	3	3	3	3	3	3	3	3
RMS WF	8.51E-09	9.55E-09	2.15E-09	1.67E-09	2.15E-09	2.00E-09	5.24E-09	5.27E-09	1.62E-08

Combining Static and Dynamic Contrast

The error budget tracks contrast (energy) contributions from many sources. Here we briefly summarize how the contrast terms are combined, and how the contrast variance is determined. Assuming a set of random, uncorrelated complex field amplitudes in the Lyot plane of a stellar coronagraph, the summed variance of the contributions at a point in the image plane is equivalent to the sum of the intensity (contrast) contributions from each field component weighted by the component variances. That is, given an aberration $\phi(\vec{x},t)$ defined as the sum of time-varying orthogonal modes $a_i(t)\phi_i(\vec{x})$,

$$\phi(\vec{x},t) = \sum_{i=1}^{N} a_i(t)\phi_i(\vec{x}) \qquad (1)$$

where the variance of the amplitudes is $\sigma_i^2 = \langle a_i^2 \rangle$, it can be shown that the mean intensity in the image plane is given by

$$\langle I(\vec{n})\rangle = \sum_{i=1}^{N} \sigma_i^2 I_i(\vec{n}) \qquad (2)$$

where $I_i(\vec{n})$ is the intensity at an image point $\vec{n}$ for the *i*th aberration. In other words, *contrast terms sum linearly; they are not combined as the root-sum-square of contrast values.* (Although from eq. 1.2 it can be shown that the wavefront errors do combine in a root-sum-square sense.) Further, it is shown that in the presence of both static contrast I_s and dynamic contrast I_d, the mean contrast level (ignoring incoherent scatter) is the sum of these terms,

$$\langle I\rangle = I_s + \langle I_d\rangle \qquad (3)$$

while the variance of the contrast includes static and dynamic cross-terms and is given by

$$\sigma_I^2 = 2I_s\langle I_d\rangle + \langle I_d\rangle^2 \qquad (4)$$

The TPF-C science requirements are tied to the engineering requirements by both $\langle I\rangle$ and σ_I. The mean intensity level, $\langle I\rangle$, determines the instrument contrast and the standard deviation, σ_I, determines the stability of the contrast.

Mask Leakage Model

The coronagraph is designed to eliminate all diffracted light in an ideal optical system. The 8th-order mask we employ has the additional advantage of being insensitive, relative to other masks, to changes in low-order aberration content[8]. Mask transmission errors caused by manufacturing errors, polarization effects (in binary masks), or wavelength dependence of mask materials, allow diffracted light to appear while increasing aberration sensitivity. The CEB employs a simple model to account for this behavior. Given an ideal electric field E_0 and a field component due to aberrations, ΔE, and similarly an ideal mask and mask transmission error, the field and mask are given by $E_{in}(x) = E_0(x) + \Delta E(x)$ and $M(x) = M_0(x) + \Delta M(x)$

The electric field passing through the mask is the product of eqs. (5) and (6),

$$E_{out} = E_{in}(x)\bullet M(x) = E_0(x)M_0(x) + \Delta E(x)M_0(x) + E_0(x)\Delta M(x) + \Delta E(x)\Delta M(x) \qquad (5)$$

The electric field at the final image plane is filtered by the Lyot stop and is given by

$$E_{image} = \left\{ \begin{matrix} E_0(x)M_0(x) + \Delta E(x)M_0(x) + \\ E_0(x)\Delta M(x) + \Delta E(x)\Delta M(x) \end{matrix} \right\} * A_{Lyot}(x) \qquad (6)$$

Here the $*$ represents the convolution operator, and $A_{Lyot}(x)$ represents the transform of the Lyot stop.

The term $E_0(x)M_0(x)$ represents the ideal field which is perfectly cancelled by band-limited masks. The term $E_0(x)\Delta M(x)$ is the static leakage – it is partially compensated by DMs when the wave front is initially set. The two terms with ΔE are represented in the dynamic error budget. The term $\Delta E(x)M_0(x)$ is the leakage of aberrations through the ideal mask. Sensitivities are given in ref. 8 for the 8th-order mask and refs. 6 and 7 for other masks.

The last term, $\Delta E(x)\Delta M(x)$, is the complex amplitude of aberrated light leaking through the mask imperfection. As shown in Fig. 2, this term appears wherever aberrations are evaluated. The contrast contribution is given by

$$C = \left(\Delta E(x) \bullet \Delta M(x) * A_{Lyot} \right)^2 \quad (7)$$

The electric field at the point of interest (in our case, 4 λ/D) is calculated from the independent contributions of Zernike terms using a Fraunhofer propagation model, and is empirically found to follow

$$\left| \Delta E(x) \right| = \left(\frac{A_{rms}}{\lambda} \right) \bullet 10^{a} \bullet \phi^{p} \quad (8)$$

where ϕ is the field angle in units of λ/D, and $A_{\rm rms}$ is the rms amplitude of the ith Zernike aberration[20]. Table 3 lists the coefficients *a* and *p* for eq. 8. The CEB carries ΔM = 5e-4 to represent the mask error at 4 λ/D.

Table 3. Coefficients for calculating aberration amplitude in the image plane.

Zernike Mode	p(x)	a(x)
2	-1.23	-3.86
3	-1.47	-0.40
4	-1.44	-0.52
5	-1.91	-2.73
6	-1.45	-0.36
7	-1.45	-0.27
8	-1.14	-3.66
9	-1.45	-0.28
10	-2.03	-2.22
11	-1.46	-0.35
12	-1.49	-0.18
13	-1.74	-2.74
14	-1.49	-0.18
15	-2.17	-1.85

Contrast from Image Motion

The linear 8th-order mask allows energy to leak through as the 8th power of image position. This applies only in the dimension of mask variations – it is insensitive to image motion in the orthogonal dimension. The leakage is a function of image offset and image jitter, both of which are specified in the CEB.

To determine the sensitivity to offset and jitter, we performed a Monte-Carlo simulation of random pointing errors, evaluating the contrast at the IWA. The contrast for a given offset Ω and jitter standard deviation σ (both expressed in milli-arcsec) is given by

$$C(\Omega, \sigma) = \left[\left(\frac{D_{prim}}{W \bullet \lambda \bullet 2.06x10^{8}} \right) \bullet \left(\Omega + N\left(0, \sigma^2\right) \right) \right]^{p} \bullet 10^{a} \quad (9)$$

where $N(0,\sigma^2)$ is a Gaussian random variable and W = 3.97 converts the pointing error into a Zernike mode 3 amplitude (for which we have evaluated contrast leakage). Calculations are performed for D = 8 m and λ=600nm. Our Fraunhofer diffraction model was used to determine *p*=8.08 and *a* = -0.69 for a mask optimized to function at IWA = 4 λ/D.

We calculate the mean and the standard deviation of the contrast for a range of offsets and random pointing noise. Then we fit the contrast standard deviation, using the least square fitting method, to a polynomial to obtain an equation for contrast vs. offset and jitter. The standard deviation of the pointing-leakage contrast is given by

$$\sigma_C = c_1\sigma^4\Omega^4 + c_2\sigma^6\Omega^2 + c_3\sigma^2\Omega^6 + c_4\sigma^8 + c_5\Omega^8 \quad (10)$$

with coefficients: c1 = 7.28e-13; c2 = 3.34e-12; c3 = 4.94e-14; c4=1.26e-12; c5=1.80e-16.

Given these polynomial coefficents and choosing Ω=0.300 mas, and σ=0.300 mas we find the standard deviation of contrast due to image motion is 3.53e-16. After applying a reserve factor of 2 to offset and jitter, we find the contrast is 9e-14. However, we find that given the DM leakage described above, the pointing error is dominated by eq. 7 not eq. 10. Mask leakage combined with 0.3 mas pointing errors is in fact the largest contrast contributor, as shown below.

6. REQUIREMENTS

Eq. 4 demands a balance between the static and dynamic contributions. As the static contribution I_s grows larger, the dynamic contribution I_d is more tightly constrained. For example for I_s = 6e-11 (our self imposed limit to keep contrast well below scattered exo-zodiacal light), we require I_d = 3e-12 to maintain σ_I = 2e-11. At present our best estimate of I_s is 3.6e-11, allowing I_d = 5.14e-12. This is the requirement for dynamic contrast contributions.

Table 4: Rolled up Dynamic Contrast Contributors

Perturbation	Contributor	Nature	Contrast	Fraction
Structural Defomation	Beam Walk	Thermal	8.29E-13	16.12%
		Jitter	6.33E-13	12.31%
	Aberrations	Thermal	3.28E-14	0.64%
		Jitter	4.43E-17	0.00%
Bending of Optics	Aberrations	Thermal	8.60E-13	16.72%
		Jitter	8.60E-13	16.72%
Pointing	Beam Walk		1.29E-12	25.10%
	Image Motion		9.04E-14	1.76%
	Mask Error		5.46E-13	10.63%
SUM			5.14E-12	

Table 4 is a roll-up of dynamic contrast contributors, including bending of the optics, beam walk across all optics, and pointing errors. The roll-up is based on allocations of engineering requirements (e.g. allowed motion of a given optic, allowed bending of an optic) applied throughout the system. Allocations were derived from extensive modeling efforts on a previous 6-meter version of TPF-C.

The largest contributor to image plane contrast is beam walk caused by pointing errors. The majority of this occurs on the first five mirrors following the secondary mirror, near the Cassegrain focus. The walk is due to 0.4 mas of pointing error that remains uncompensated by the secondary mirror. (Recall that the secondary corrects up to 4 mas of rigid body pointing, but 0.4 mas is at frequencies beyond the secondary mirror control bandwidth.) The first two folds and the first off-axis parabola have 'Super Fold' and 'Super OAP' PSDs (Table 2), while the cylindrical optics are about 2.5 times worse. To reduce the beam walk, we must adopt a combination of better pointing and better optical surfaces. Note that if the secondary mirror is not used in the pointing control loop, and if rigid body pointing stability is $\sigma = 4$ mas, there is 10x more beam walk on these optics, resulting in contrast of 1.3e-10 (and the overall dynamic contrast going to 1.67e-10).

The single largest contrast term in the error budget is the 'Mask Error' term at the bottom of Table 4. As noted above, this term is the leakage of light that is offset by 0.3 mas with 0.3 mas random pointing error, through a mask with a 5e-4 transmission error at 4 λ/D. We expect that it will be challenging to build a mask to this level of precision. The leakage falls off as the square of the pointing error, so a reduction in pointing error will relax the mask requirement.

Bending of optics is mainly bending of the primary mirror. The 8^{th}-order mask filters out low-order bending up through Z10 (trefoil), but higher order modes (Z11, spherical aberration and above) scatter light at much lower aberrations levels. Figure 5 shows the requirements on the primary mirror wave front bending modes (surface deformation is 2x smaller). The major contributors are 0.2 nm r.m.s. of coma (contrast = 2.7e-13), and 0.005 nm of Z11 and Z12 (3.7e-13 combined). We assume that bending of the secondary is 4x smaller than the primary, and all other optics bend 8x less than the primary. As aberration leakage scales as the 4^{th} (Z3-Z10) or 2^{nd} (Z11 and higher) power of aberration amplitude, the downstream optics play only a small role in the overall contrast. Mask errors combined with the small primary mirror aberrations do not significantly increase the contrast. At the present time we have placed identical requirements on thermal- and jitter-induced bending but will adjust this as our model fidelity improves.

Finally, structural deformation (the motion of optics relative to one another, with the PM fixed) contributes both beam walk and aberrations. The beam walk is a far worse effect, again dominated by optics M3-M7. Thermal motions of the secondary mirror are corrected to the precision of the laser metrology truss (25 nm per beam r.m.s.); this results in ~ 20 nm of motion along the line-of-sight, and 65 nm of lateral motion. With the system stop placed at the DM, most of the beam motion occurs on the secondary mirror but it is only a small contrast contributor because the PSD has not scaled with the optic diameter relative to the downstream optics. Optics between the secondary and coronagraph mask are restricted to thermally-induced motions of 10 nrad and 100 nm in tilt and translation, respectively. These motions are partially compensated by the secondary mirror. Within the bandwidth of the fine steering mirror, the motions are 10 nrad and 10 nm. Higher frequency (uncompensated) motions are restricted to 1 nrad and 1 nm.

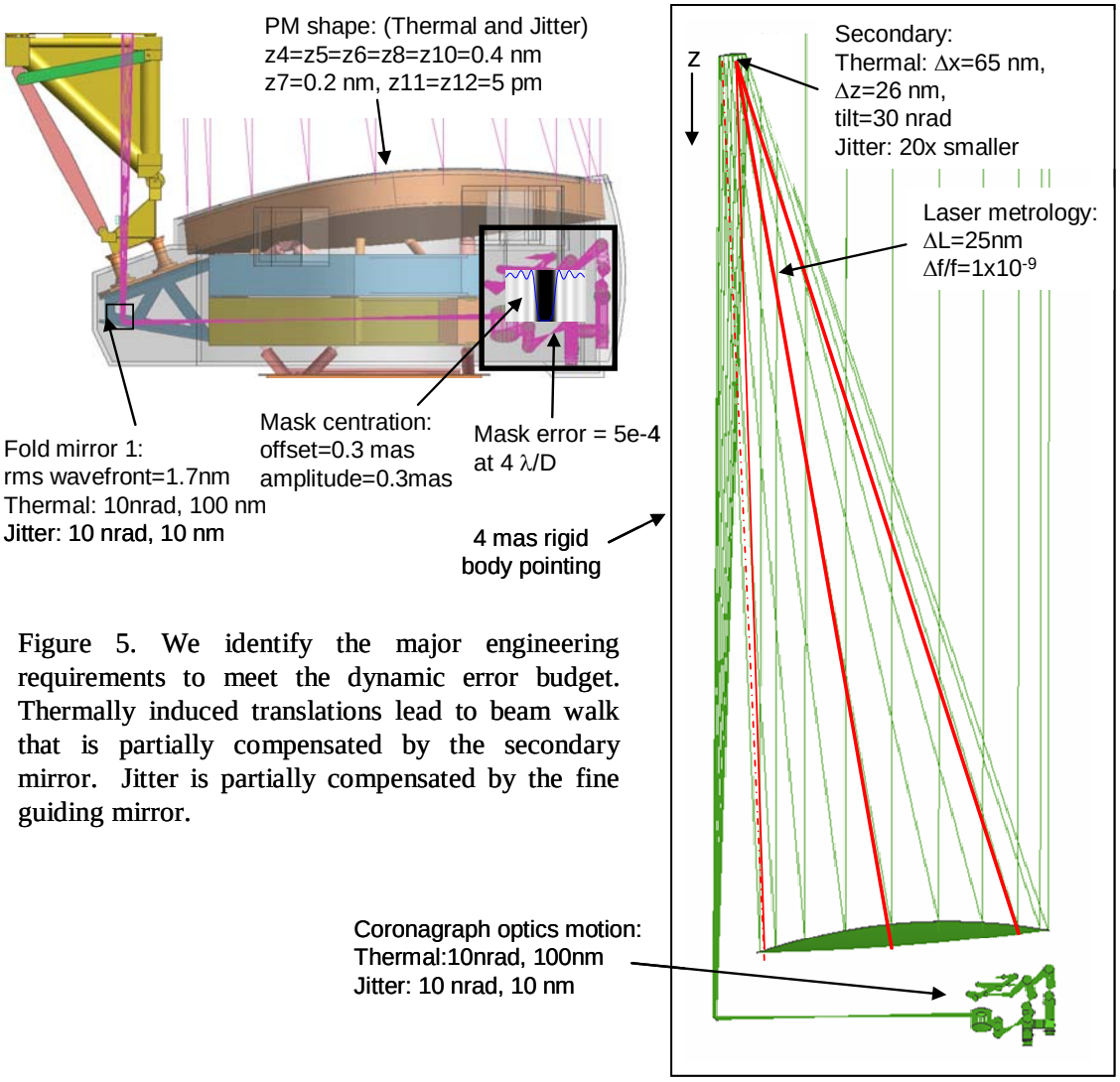

Figure 5. We identify the major engineering requirements to meet the dynamic error budget. Thermally induced translations lead to beam walk that is partially compensated by the secondary mirror. Jitter is partially compensated by the fine guiding mirror.

7. CONCLUDING REMARKS

We are working to add new modeling capabilities and to validate those capabilities in testbeds. Required models not presently in hand include: coating non-uniformities, high-contrast stray-light and scattered light models validated, and wave-front sensing and control models that demonstrate the ability to identify speckles at the 1e-11 level. Presently we have no models – and virtually no data – on coating non-uniformities related to large-scale anisotropies in the deposition process. These effects might limit the useful optical bandwidth because the wavelength response of the phase-based wave front control system is likely to be different from the wavelength dependence of the amplitude non-uniformities. Scattered light models treat forward-scattered light as being uniformly shifted in phase relative to the non-scattered beam. This approximation must be validated or superseded by new models. Stray-light (multiply-reflected from baffles, edges, etc.) is calculated using standard stray-light software but the accuracy of the calculations at the 1e-11 level has never been validated.

Mission modeling simulations have shown that planet detection efficiency benefits from increased sensitivity (beyond our current baseline of 1e-10) in spite of the increased integration times required to improve sensitivity. We are

currently considering a change to our requirements that will enable deeper searches by a factor of 2 or 3. This will have a factor of 2-3 effect on the dynamics requirements because the dynamic errors (in particular beam walk and high-order primary mirror bending) scale as the square of optics motion and bending, while eq. 4 shows that in the presence of significant static errors, the contrast stability scales as the square root of the dynamic errors.

ACKNOWLEDGEMENTS

We wish to acknowledge the technical contributions of P. Mouroulis, P. Dumont, K. Balasubramanian, and P. Lawson to this body of work. This work was carried out at the Jet Propulsion Laboratory, California Institute of Technology, under contract with the National Aeronautics and Space Administration.

REFERENCES

1. Ford, V.G., et al, "The Terrestrial Planet Finder Coronagraph 2005: Overview of System Design Studies and Technology Development," Proc. SPIE Vol. 5905 (2005).
2. Brown, R.A., "Single Visit Photometric and Obscurational Completeness," ApJ 624, pp. 1010-1024 (2005).
3. Kuchner, M.J., and Traub, W.A., "A Coronagraph with a Band-Limited Mask for Finding Terrestrial Planets," ApJ 570, pp. 900-908 (2002).
4. Trauger, J.T., et al, "Coronagraph Contrast Demonstrations with the High Contrast Imaging Testbed," Proc. SPIE Vol. 5487, pp. 1330-1337 (2004).
5. Brown, R.A., "Obscurational Completeness," ApJ 607, pp. 1003-1013 (2004).
6. Green, J.J., & Shaklan, S.B., "Optimizing Coronagraph Performance Designs to Minimize Their Contrast Sensitivity to Low-Order Optical Aberrations," Proc. SPIE Vol. 5170, pp. 25-37 (2003).
7. Green, J.J., & Shaklan, S.B., "The Sensitivity of Shaped Pupil Coronagraphs to Optical Aberrations," Proc. SPIE Vol. 5487, pp. 1358-1368 (2004).
8. Shaklan, S.B., & Green, J.J., "Low-Order Aberration Sensitivity of Eighth-Order Coronagraph Masks," ApJ (in press) 2005.
9. Noecker, M.C., "TPF Coronagraph Wavefront Changes Due to Beam Walk," Proc. SPIE Vol. 5905 (2005).
10. Kuchner, M.J., Crepp, J., & Ge, J., "Finding Terrestrial Planets using 8th-order Image Masks," ApJ (in press) 2005.
11. Laskin, R.A., "SIM Technology Development: Light at the End of the Tunnel," SPIE Vol. 4852, pp. 16-32 (2002)
12. Shaklan, S.B., et al, "Metrology System for the Terrestrial Planet Finder Coronagraph," Proc. SPIE Vol 5528, pp. 22-31 (2004).
13. MACOS (Modeling and Analysis of Controlled Optical Systems) Manual, JPL Document.
14. Howard, J.M., et al, "Optical Design Considerations for the Terrestrial Planet Finder Coronagraph Mission: Optical Telescope Assembly," Proc. SPIE Vol. 5874 (2005).
15. Mouroulis, Z. & Shaklan, S, SSS paper
16. Halverson, P.G., et al, "Measurement of Wavefront Phase Delay and Optical Density in Apodized Coronagraphic Mask Materials," Proc. SPIE Vol. 5905 (2005).
17. Lay, O.P., et al, "Coronagraph Mask Tolerances for Exo-Earth Detection," Proc. SPIE Vol. 5905 (2005).
18. Balasubramanian, K., et al, "Polarization compensating protective coatings for TPF-Coronagraph optics to control contrast degrading cross polarization leakage," Proc. SPIE Vol. 5905 (2005).
19. Breckinridge, J.B., & Oppenheimer, B.R., "Polarization Effects in Reflecting Coronagraphs for White-Light Applications in Astronomy," ApJ 600, pp. 1091-1098 (2004)
20. Noll, R.J., "Zernike Polynomials and Atmospheric Turbulence." J. Opt. Soc Am. 66, pp. 207-211 (1976).